

A Bayesian Analysis of Large Discrete Graphical Models

Anwesa Bhattacharyya*

Department of Statistics, University of Michigan

and

Yves Atchade†

Department of Statistics, Boston University

October 21, 2019

*anwebha@umich.edu

†atchade@bu.edu

⁰ *This work is partially supported by the NSF grant DMS 1513040. MSC 2010 subject classifications: Primary 62F15, 60K35; secondary 60K35*

Abstract

This work introduces a Bayesian methodology for fitting large discrete graphical models with spike-and-slab priors to encode sparsity. We consider a quasi-likelihood approach that enables node-wise parallel computation resulting in reduced computational complexity. We introduce scalable MCMC algorithms for sampling from the quasi-posterior distribution which enables variable selection and estimation simultaneously. We present extensive simulation results to demonstrate scalability and accuracy of the method. We also analyze the 16 Personality Factors (PF) dataset to illustrate performance of the method. A Matlab implementation of the algorithms is also provided as support material.

Keywords: Discrete graphical models, networks, High-dimensional Bayesian inference, Spike-and-slab priors, Markov Chain Monte Carlo

1 Introduction

In this paper we are primarily interested in model-based inference of large undirected networks from observed data at each node, in settings where the data can take only finitely many values. This is motivated by the widespread availability of this type of data in areas of psychology, image processing, computer science, social sciences, bio-informatics, to name a few. For instance, Banerjee et al. (2008) used an Ising model to find association between US senators from their binary voting records. Ekeberg et al. (2013) used a Potts model to predict contact between amino acids in protein chains. In Epskamp et al. (2017, 2018), the authors worked the reader through statistical procedures for estimating psychological networks in personality research. The Ising model Ising (1925) was originally formulated in the Physics literature as a simple model for interacting magnetic spins on a lattice. The Potts model is a generalization of the Ising model in which spins can take more than two values with more complex dependencies. These models are widely used in the applications for teasing out direct and undirected dependencies between large collections of variables. The purpose of this work is to construct robust and scalable bayesian procedures for fitting these models.

Bayesian statistics has two built-in features that are in growing demand in the applications: a) the ability to incorporate existing knowledge in new data analysis (Greenfield et al. (2013); Studham et al. (2014); Peng et al. (2013)), and b) a simple mechanism for uncertainty quantification in the inference. However these features come at a hefty computational price: most existing Bayesian methods for fitting graphical models do not scale well as the number of nodes in the graph grows, despite the recent progress with Gaussian graphical models (Dobra et al. (2011); Khondker et al. (2013); Peterson et al. (2015); Banerjee and Ghosal (2015)). The computational challenge only intensifies when dealing with discrete graphical models (Ising and Potts models). Here a full Bayesian treatment leads to the so-called doubly-intractable posterior distributions for which specialized MCMC al-

gorithms are needed (Zhou and Schmidler (2009); Murray et al. (2006); Lyne et al. (2015)). However these algorithms do not scale well when dealing with large graphical models.

In the frequentist literature there is a long history of fitting discrete graphical models using (quasi/pseudo)-likelihood methods instead of the full likelihood (dating back at least to Besag (1974); see also Guyon (1995)). In fact, quasi-likelihood methods have become the de facto approach in the frequentist literature when dealing with large graphical models (Meinshausen and Buhlmann (2006); Höfling and Tibshirani (2009); Ravikumar et al. (2010); Guo et al. (2015); Roy et al. (2017)).

In the Bayesian framework, the idea of using a non-likelihood function to carry out inference has been adopted at a more slower pace, but is currently in growing popularity (Chernozhukov and Hong (2003); Jiang and Tanner (2008); Liao and Jiang (2011); Yang and He (2012); Kato (2013); Li and Jiang (2014); Atchade (2017, 2019)). For instance in Atchade (2019) a quasi-likelihood approach is developed to fit Gaussian graphical models in the Bayesian framework at a scale unmatched by fully Bayesian alternatives. The crux of the method is the use of a product-form pseudo-likelihood function (as used in the frequentist literature) that makes it possible to split the resulting quasi-posterior distribution into a product of linear regression Bayesian posterior distributions. Significant reducing in computational costs is then achieved by deploying this approach on a multi-core computer system. In this paper we extend the same strategy to the analysis of discrete graphical models.

We focus on settings where the underlying network is sparse. Under this assumption, the inference problem is commonly approached by introducing an auxiliary selection variable that represents the structure of the network. We then follow a well-established practice in the Bayesian literature that imposes a spike-and-slab prior distribution jointly on the network parameter and the network structure (Mitchell and Beauchamp (1988); George and McCulloch (1997); Narisetty and He (2014); Atchade and Bhattacharyya (2019)). More

precisely, we actually follow here the sparse model spike and slab prior of Atchade and Bhattacharyya (2019), a computationally efficient version of the standard spike and slab prior of George and McCulloch (1997).

In summary, in this paper we put together a scalable Bayesian methodology for fitting high-dimensional Potts or Ising models. Our method simultaneously estimates the model parameters and the underlying structure of the graph. We develop scalable Markov Chain Monte Carlo (MCMC) algorithms that can be implemented in parallel thus significantly reducing the computational cost of the method. Our method not only provides us with robust point estimates but also gives us credible intervals for the model parameters. We extensively tested the method using simulated data, and illustrates its practical applicability using an example from personality research.

The rest of the article is organized as follows: Section 2 introduces the methodology. In section 3, we propose two scalable MCMC algorithms to deal with the resulting quasi-posterior distribution. Section 4 illustrates the performance of our method through simulation results. Finally, in section 5, we present an application of our method in the context of psychological data through the analysis of the 16 Personality Factors (16PF) dataset.

2 Quasi-posterior distribution of the Potts model under spike and slab prior

An m -colored Potts model parametrized by a sparse symmetric matrix θ is a probability mass function on $\mathcal{Z} = \{0, 1, \dots, m - 1\}^p$ given by

$$f(z_1, \dots, z_p | \theta) = \frac{1}{\Psi(\theta)} \exp \left\{ \sum_{r=1}^p \theta_{rr} C(z_r) + \sum_{r=1}^p \sum_{j < r}^p \theta_{rj} C(z_r, z_j) \right\}. \quad (1)$$

Here $\Psi(\theta) = \sum_{z \in \mathcal{Z}} \exp \left\{ \sum_{r=1}^p \theta_{rr} C(z_r) + \sum_{r=1}^p \sum_{j < r}^p \theta_{rj} C(z_r, z_j) \right\}$ is the normalizing constant. The mean field function $C(\cdot)$ describes the marginal information on z_r while the coupling function $C(\cdot, \cdot)$ as suggested by the name describes the interaction between z_r and z_j . A special case of (1) is the Ising Model where m is 2, and hence $\mathcal{Z} = \{0, 1\}^p$. In case of the Ising model the mean field and the coupling functions are typically taken as identity ($C(z_r) = z_r$) and multiplicative ($C(z_r, z_j) = z_r z_j$) respectively.

The problem of interest in this work is the estimation and recovery of the sparse matrix θ based on n sample observations $\{z^i\}_{i=1}^n$, where $z^i = (z_1^i, \dots, z_p^i) \in \mathcal{Z}$ is the i th observation. We use $Z \in \{0, \dots, m-1\}^{n \times p}$ to denote the matrix of observations, where the i -th row of Z is z^i . The likelihood of θ can then be expressed as

$$\mathcal{L}^n(\theta|Z) = \prod_{i=1}^n f(z^i|\theta) = \prod_{i=1}^n \frac{1}{\Psi(\theta)} \exp \left\{ \sum_{r=1}^p \theta_{rr} C(z_r^i) + \sum_{r=1}^p \sum_{j < r}^p \theta_{rj} C(z_r^i, z_j^i) \right\}.$$

In a high-dimensional setting (typically $p > n$, $\frac{\log(p)}{n} \rightarrow 0$), likelihood based inference on θ is computationally intractable because of the normalization constant $\Psi(\theta)$. Note that, the number of summands in the normalizing constant $\Psi(\theta)$ is exponential in p , and quickly blows up for even moderate values of p .

2.1 Quasi(Pseudo)-likelihood

Following an approach widely adopted in the high-dimensional frequentist literature, we explore the use of quasi(pseudo)-likelihoods in the Bayesian treatment of discrete graphical models. The conditional distribution for the r th node (given all other nodes) in a Potts

model for the i_{th} observation z^i can be written as

$$f(z_r^i | z_{\setminus r}^i, \theta_r) = \frac{1}{\Psi_r^i(\theta_r)} \exp \left\{ \theta_{rr} C(z_r^i) + \sum_{j \neq r} \theta_{rj} C(z_r^i, z_j^i) \right\}, \quad (2)$$

where $z_{\setminus r}^i = (z_1^i, \dots, z_{r-1}^i, z_{r+1}^i, \dots, z_p^i)'$ and $\theta_r = (\theta_{r1}, \dots, \theta_{rp})'$ is the r_{th} column of θ . The normalizing constant of this conditional distribution is given by

$$\Psi_r^i(\theta_r) = \sum_{s=0}^{m-1} \exp \left(\theta_{rr} C(s) + \sum_{j \neq r} \theta_{rj} C(s, z_j^i) \right).$$

Computing $\Psi_r^i(\theta_r)$ requires $O(p \times m)$ units of operations and hence is scalable when m is small. We denote the r_{th} conditional log-likelihood as

$$\ell_r^n(\theta_r | Z) = \sum_{i=1}^n \left[\theta_{rr} C(z_r^i) + \sum_{j \neq r} \theta_{rj} C(z_r^i, z_j^i) - \log \left(\Psi_r^i(\theta_r) \right) \right].$$

Following Meinshausen and Buhlmann (2006); Ravikumar et al. (2010), we consider the log pseudo-likelihood of θ given by

$$\ell^n(\theta | Z) = \sum_{r=1}^p \ell_r^n(\theta_r | Z). \quad (3)$$

Note that the ability to write the log pseudo-likelihood $\ell^n(\theta | Z)$ as a sum of log conditional likelihoods $\ell_r^n(\theta_r | Z)$ allows us to transform the inference on $\theta \in \mathbb{R}^{p \times p}$ into p separable sub-problems on \mathbb{R}^p . Parallel treatment of each of these regression problems when deploying a multi-core computer increases computational efficiency but comes at a cost of loss in symmetry in the estimated matrix θ . We get two estimates for each component θ_{ij} from the computations involving nodes i and j respectively. Following Meinshausen and Buhlmann (2006) we resolve this issue at the post-inference stage by taking an aggregate of the two estimates which shall be discussed in details in the later sections.

2.2 Spike and slab prior

To take advantage of the factorized form of the pseudo-likelihood function from (3) we will assume in our prior distribution that the columns of θ are independent. We note that it is a common practice in Bayesian data analysis to ignore unknown dependence structure among parameters in the prior distribution when dealing with multivariate parameters. These dependences are then learned from the data in the posterior distribution. As mentioned before, the lack of symmetry is dealt with at the post-inference stage.

As a prior distribution for θ_r we propose to use a relaxed form of the spike and slab prior (Mitchell and Beauchamp (1988), George and McCulloch (1997)). More specifically, for each parameter $\theta_r \in \mathbb{R}^p$, $r = 1, \dots, p$, we introduce a selection parameter $\delta_r = (\delta_{r1}, \dots, \delta_{rp}) \in \Delta$, where $\Delta = \{0, 1\}^p$. We assume that the component of δ_r have independent Bernoulli prior distributions, so that the joint distribution of δ_r writes

$$\omega_{\delta_r} = \prod_{j=1}^p q^{\delta_{rj}} (1-q)^{1-\delta_{rj}} ; q = p^{-(u+1)} ; u > 0 \quad (4)$$

where u is a hyper-parameter. The conditional distribution of θ_r given δ_r is given by

$$\begin{aligned} \theta_{rj} | \{\delta_{rj} = 1\} &\sim \mathbf{N}(0, \rho); \rho > 0 \\ \theta_{rj} | \{\delta_{rj} = 0\} &\sim \mathbf{N}(0, \gamma); \gamma > 0, \end{aligned} \quad (5)$$

We introduce the notations $\theta_{r\delta_r} = (\theta_{rj} \text{ s.t. } \delta_{rj} = 1) \in \mathbb{R}^{\|\delta_r\|_1}$, $\delta_r^c = 1 - \delta_r$, $\|z\|_1 = \sum_{j=1}^p |z_j|$ and $\|z\|_2 = \sqrt{\sum_{j=1}^p z_j^2}$. Using this notation, and writing $\delta = (\delta_1, \dots, \delta_p)$, $\theta = (\theta_1, \dots, \theta_p)$, the joint prior distribution of $(\delta, \theta) \in \Delta^p \times \mathbb{R}^{p \times p}$ is given by

$$\pi(\delta, d\theta) = \prod_{r=1}^p \pi(\delta_r, d\theta_r).$$

The prior distribution $\pi(\delta_r, d\theta_r)$ on $\Delta \times \mathbb{R}^p$ can be written as

$$\pi(\delta_r, d\theta_r) \propto \omega_{\delta_r} (2\pi\rho)^{-\frac{\|\delta_r\|_1}{2}} (2\pi\gamma)^{\frac{\|\delta_r\|_1}{2}} \exp\left(-\frac{1}{2\rho} \sum_{j: \delta_{rj}=1} \theta_{rj}^2 - \frac{1}{2\gamma} \sum_{j: \delta_{rj}=0} \theta_{rj}^2\right) d\theta_r. \quad (6)$$

2.3 Quasi-posterior distribution

Following Atchade and Bhattacharyya (2019), we combine the prior distribution in (6) together with the pseudo-likelihood $\ell_r(\cdot|Z)$ and consider the quasi-posterior distribution for the r -th column of θ on $\Delta \times \mathbb{R}^p$ given by

$$\Pi_n(\delta_r, d\theta_r|Z) \propto \omega_{\delta_r} \left(\frac{\sqrt{\gamma}}{\sqrt{\rho}}\right)^{\|\delta_r\|_1} \exp\left(\ell_r^n(\theta_{r\delta_r}|Z) - \frac{1}{2\rho} \sum_{j: \delta_{rj}=1} \theta_{rj}^2 - \frac{1}{2\gamma} \sum_{j: \delta_{rj}=0} \theta_{rj}^2\right) d\theta_r. \quad (7)$$

Note the use of $\theta_{r\delta_r}$ (the sparsified version of θ_r) in the quasi-likelihood. Although we use the same standard Gaussian-Gaussian spike-and-slab prior (as in for instance George and McCulloch (1997), Narisetty and He (2014)), the quasi-posterior in (7) differs from those considered in the aforementioned paper due to the sparsification of $\theta_{r\delta_r}$ in the quasi-likelihood. The idea was introduced in Atchade and Bhattacharyya (2019) to facilitate computation and more closely approximate the quasi-posterior distribution obtained from spike-and-slab with point-mass at the origin. The contraction properties of (7) are analyzed in Atchade and Bhattacharyya (2019). We multiplicatively combine these p quasi-posterior distributions to obtain the full quasi-posterior distribution on (δ, θ) given by

$$\Pi_n(\delta, d\theta|Z) = \prod_{r=1}^p \Pi_n(\delta_r, d\theta_r|Z). \quad (8)$$

2.4 Choice of hyper-parameters

The behavior of (7) depends by and large on the choice of the hyper-parameter γ, ρ and u . We refer the readers to Atchade and Bhattacharyya (2019) for a detailed discussion. In our algorithms we set q in (4) at $q = \frac{1}{p^{1+u}}$, for some constant $u > 0$. We have found that the inference is typically very robust to any choice of u between 1 and 2.

The hyper-parameter γ is the prior variance of the inactive component, whereas ρ is the prior variance of the active components. We follow Atchade and Bhattacharyya (2019), and for positive constants c_0, c_1 , choose

$$\gamma = \frac{c_0}{\max(n, p)}, \quad \text{and} \quad \rho = c_1 \sqrt{\frac{n}{\log(p)}}.$$

2.5 Post estimation symmetrization

As mentioned above our procedure can lead to two different set of estimates $\hat{\theta}_{ij}$ and $\hat{\theta}_{ji}$ for the same parameter θ_{ij} . For the sake of interpretation it is useful to provide a single estimate and credible interval. We propose a post-estimation symmetrization resulting in a singular estimate

$$\tilde{\theta}_{ij} = \frac{\hat{\theta}_{ij} + \hat{\theta}_{ji}}{2}. \tag{9}$$

Similarly, the credible region corresponding to the parameter θ_{ij} is constructed as union of the 95% credible intervals θ_{ij} and θ_{ji} . Taking the union is a conservative approach as opposed to taking the intersection. However it always provides a concrete interval or set unlike the intersection in which case the credible intervals may be too short or in some cases even result in null set. A more direct inference on the presence of edge between nodes i and j can be made from the indicator variable δ_{ij} . In the same spirit as above we estimate δ_{ij} using

$$\tilde{p}_{ij} = P(\text{edge between node } i \text{ and } j | Z) = \frac{1}{2} \left(\hat{P}(\delta_{ij} = 1 | Z) + \hat{P}(\delta_{ji} = 1 | Z) \right). \quad (10)$$

3 MCMC Sampling Algorithms

In this section we shall discuss in details the construction of Markov Chain Monte Carlo (MCMC) algorithms to draw Monte Carlo samples from the posterior distribution (8). By virtue of independence, it is enough to draw sample for each of the joint variable (θ_r, δ_r) . Large efficiency gain is possible by performing these simulations in parallel. In general we adopt a Metropolis-Hastings within Gibbs approach to create our samplers.

We describe in Section 3.1 a general Metropolis Adjusted Langevin Algorithm (MALA) to sample from (8). In case of Ising model, one can also take advantage of the fact that the conditional distributions are logistic regression models and employ the Polya-Gamma(PG) sampler of Polson et al. (2013) for sampling (Section 3.2). We compare the two schemes in Section 4.1.

3.1 A Metropolis Adjusted Langevin sampler

The algorithm updates the active components $\theta_{r\delta_r}$ given $(\delta_r, \theta_{r\delta_r^c})$, then updates the inactive components $\theta_{r\delta_r^c}$ given $(\delta_r, \theta_{r\delta_r})$, and finally updates δ_r given (θ_r) . Here we have used the notations $\theta_r = [\theta_{r\delta_r}, \theta_{r\delta_r^c}]$, where $\theta_{r\delta_r}$ regroups the components of θ_r for which $\delta_{rj} = 1$, and $\theta_{r\delta_r^c}$ regroups the remaining components. We refer the reader to Robert and Casella (2004); Liu (2001) for an introduction to basic MCMC algorithms.

Update of active parameters

Suppose that δ_r is such that $0 < \|\delta_r\|_1 < p$. We update $\theta_{r\delta_r}$ by a Metropolis Adjusted

Langevin Algorithm (Atchade (2006)). Other algorithms including Hamiltonian Monte Carlo could be used as well. We define

$$h(\delta_r, \theta_r; z) = \left[\ell_r^n(\theta_{r\delta_r}|z) - \frac{1}{2\rho} \|\theta_{r\delta_r}\|_2^2 - \frac{1}{2\gamma} \|\theta_{r\delta_\xi}\|_2^2 \right]. \quad (11)$$

The function $\theta_r \rightarrow h(\delta_r, \theta_r; z)$ has a gradient given by

$$\nabla_{\theta_r} h_\gamma(\delta_r, \theta_r; z) = \nabla_{\theta_{r\delta_r}} \ell_r^n(\theta_{r\delta_r}|z) - \frac{1}{\rho} \theta_{r\delta_r} - \frac{1}{\gamma} \theta_{r\delta_\xi}.$$

Following (Atchade (2006)), we further truncate the gradient by introducing

$$G(\delta_r, \theta_r; z) \stackrel{\text{def}}{=} \frac{c}{c \vee \|\nabla_{\theta_r} h(\delta_r, \theta_r; z)\|_2} \nabla_{\theta_r} h(\delta_r, \theta_r; z), \quad (12)$$

for some positive constant c , where $a \vee b = \max(a, b)$. We update (one at the time) the selected components of θ_r as follows. Given j such that $\delta_{rj} = 1$, we propose

$$\theta_{rj}^{prop} | \theta_r \sim \mathbf{N} \left(\theta_{rj} + \frac{\sigma}{2} [G(\delta_r, \theta_r; z)]_j, \sigma^2 \right), \quad (13)$$

where σ is some constant step size and $[G(\delta_r, \theta_r; z)]_j$ represents the j th component of $G(\delta_r, \theta_r; z)$. Let $g(\theta_{rj}^{prop} | \theta_r)$ denote the density of the proposal distribution in (13). We also define $\theta_r^{prop} = [\theta_{r1}, \dots, \theta_{r(j-1)}, \theta_{rj}^{prop}, \theta_{r(j+1)}, \dots, \theta_{rp}]$ and the acceptance probability as

$$\text{Acc}_{rj} = \min \left(1, \frac{g(\theta_{rj} | \theta_r^{prop})}{g(\theta_{rj}^{prop} | \theta_r)} \times \frac{\Pi_n(\delta_r, \theta_r^{prop} | Z)}{\Pi_n(\delta_r, \theta_r | Z)} \right). \quad (14)$$

With probability Acc_{rj} we set $\theta_{rj} = \theta_{rj}^{prop}$, and with probability $1 - \text{Acc}_{rj}$, we do nothing. In our simulations the step size σ is kept constant. Alternatively, it can also be updated for each θ_{rj} in the spirit of an adaptive MCMC scheme if so desired.

Finally we note that, under sparse prior the number of active parameters in each node is

small. Hence the active parameters at a node can be updated one by one without loss in computational efficiency.

Independent update for inactive parameters

Note that for the stated posterior distribution 7, given δ_r , the inactive components $\theta_{r\delta_r^c}$ can be updated from their full conditional distribution given by

$$\theta_{r\delta_r^c} \sim \mathbf{N}(\mathbf{0}, \gamma I_{p-\|\delta_r\|_1}). \quad (15)$$

Bernoulli sampler for selection parameters

Equation (7) is used to derive the one by one Gibbs update of the δ_{rj} 's. For each $j = 1, \dots, p$, we define $\check{\delta}_r = (\delta_{r1}, \dots, \delta_{r(j-1)}, \delta_{rj}^c, \delta_{r(j+1)}, \dots, \delta_{rp})$ and set

$$\tau_{rj} = \min \left(1, \frac{\left(\frac{q}{1-q}\right)^{\|\check{\delta}_r\|_0} \left(\frac{\gamma}{\rho}\right)^{\frac{\|\check{\delta}_r\|_0}{2}} e^{h(\check{\delta}_r, \theta_r; z)}}{\left(\frac{q}{1-q}\right)^{\|\delta_r\|_0} \left(\frac{\gamma}{\rho}\right)^{\frac{\|\delta_r\|_0}{2}} e^{h(\delta_r, \theta_r; z)}} \right) \quad (16)$$

We change δ_{rj} to δ_{rj}^c based on a flip of probability τ_{rj}

The overall MCMC algorithm, hereafter referred to as MALA can be summarized as follows.

Algorithm 1. MALA sampler

For each node $r \in \{1, \dots, p\}$ do the following.

1. Initialize with $(\theta_r^{(0)}, \delta_r^{(0)})$
2. At the t -th iteration, given $\delta_r^{(t-1)} = \check{\delta}$ and $\theta_r^{(t-1)} = \check{\theta}$, do
 - (a) For each j such that $\check{\delta}_j = 1$, we update $\check{\theta}_j$ using the MALA algorithm described in (13) and (14).
 - (b) Update $\check{\theta}_{\delta_r^c} \sim \mathbf{N}(0, \gamma I_{p-\|\check{\delta}\|_0})$
 - (c) Set $\theta_r^{(t)} = \check{\theta}$. For each j in $\{1, \dots, p\}$, we update $\check{\delta}_j$ based on a binary flip of probability τ_{rj} as defined in (16). Set $\delta_r^{(t)} = \check{\delta}$.

3.2 A Polya-Gamma sampler for Ising models

The Polya-Gamma sampler is a data-augmentation technique which introduces latent Polya-gamma variables to obtain an efficient Gibbs sampler for Bayesian logistic regression (Polson et al. (2013)). To see how this is used here, note that the conditional posterior of the active parameters for the r th node is

$$\Pi_n(\theta_{r\delta_r} | \delta_r, \theta_{r\delta_r^c}; Z) \propto \exp \left(\ell_r^n(\theta_{r\delta_r} | Z) - \frac{1}{2\rho} \sum_{j:\delta_{rj}=1} \theta_{rj}^2 \right), \quad (17)$$

which is the same as the posterior distribution in a logistic regression of variable z_r over the variables z_j for which $\delta_{rj} = 1$, $j \neq r$, using all available data samples. Given r, δ_r , we write $x(r)_{\delta_r}^{(i)} = (z_1^{(i)}, \dots, z_{r-1}^{(i)}, 1, z_{r+1}^{(i)}, \dots, z_p^{(i)})_{\delta_r} \in \{0, 1\}^{\|\delta_r\|_1}$, $Z_r = (z_r^{(1)}, \dots, z_r^{(n)})' \in \{0, 1\}^n$ and use $X(r)_{\delta_r} \in \{0, 1\}^{n \times \|\delta_r\|_1}$ to denote the matrix of n observations $\{x(r)_{\delta_r}^{(i)}\}_{i=1}^n$.

Hence to sample from (17) we follow a Gibbs update of first drawing independently Polya-Gamma random variables using

$$W_i | \theta_{r\delta_r} \sim \mathbf{PG}(1, |\langle x(r)_{\delta_r}^{(i)}, \theta_{r\delta_r} \rangle|); \quad i = 1, \dots, n \quad (18)$$

Note that $\langle a, b \rangle$ denotes the inner product between two vectors a, b . The second step is to update $\theta_{r\delta_r}$ given these Polya-Gamma variables using

$$\theta_{r\delta_r} \sim \mathbf{N}(\mu, \Sigma) \quad (19)$$

$$\mu = \Sigma \left(X(r)_{\delta_r}^T (Z_r - \frac{1}{2} \mathbf{1}_n) \right) \quad (20)$$

$$\Sigma = \left(X(r)_{\delta_r}^T \Omega X(r)_{\delta_r} + \frac{1}{\rho} I_{\|\delta_r\|_0} \right)^{-1} \quad (21)$$

$$\Omega = \text{diag}(W_1, \dots, W_n) \quad (22)$$

Independent update for inactive parameters

As in (15) given δ_r , the inactive components $\theta_{r\delta_r^c}$ can be updated independently and simultaneously from $\mathbf{N}(\mathbf{0}, \gamma I_{p-\|\delta_r\|_1})$

Bernoulli sampler for selection parameters

As before, (7) is used to derive the one by one Gibbs update of the δ_{rj} 's. For the Polya-Gamma (PG) sampler, the calculations of the Bernoulli probability of the update can be simplified. For each $j = 1, \dots, p$, we define

$$\begin{aligned} \tau_{rj} = & \log\left(\frac{1-q}{q}\right) - \frac{1}{2} \log\left(\frac{\gamma}{\rho}\right) + \frac{1}{2} \left(\frac{1}{\rho} - \frac{1}{\gamma}\right) \theta_{rj}^2 - \frac{1}{2} \left([X(r)]'_{\cdot j} \Omega [X(r)]_{\cdot j}\right) \theta_{rj}^2 \\ & - \theta_{rj} \left\langle [X(r)]_{\cdot j}, \left(Z_r - \frac{1}{2} \mathbf{1}_n\right) \right\rangle - \left\langle \theta_{r\delta_r}, [X(r)]'_{\cdot j} \Omega X(r)_{\delta_r} \right\rangle \quad (23) \end{aligned}$$

where $X(r)$ denotes the full matrix $X(r)_{\mathbf{1}_p}$ and $[X(r)]_{\cdot j}$ denotes the j th column of $X(r)$.

When $\delta_{rj} = 1$ we flip it to 0 with probability $\min(1, e^{\tau_{rj} + \theta_{rj} [X(r)]'_{\cdot j} \Omega [X(r)]_{\cdot j}})$. On the other hand if $\delta_{rj} = 0$ we flip it to 1 with probability $\min(1, e^{-\tau_{rj}})$.

The Polya-Gamma MCMC algorithm (hereafter PG sampler) can be summarized as follows.

Algorithm 2. PG sampler

For each node $r \in \{1, \dots, p\}$ do the following.

1. Initialize with $(\theta_r^{(0)}, \delta_r^{(0)})$
2. At the t -th iteration, given $\delta_r^{(t-1)} = \check{\delta}$ and $\theta_r^{(t-1)} = \check{\theta}$, do
 - (a) we update $\check{\theta}_{\check{\delta}}$ using the Polya-Gamma algorithm described in (18 - 22).
 - (b) Update $\check{\theta}_{\check{\delta}^c} \sim N(0, \gamma I_{p-\|\check{\delta}\|_0})$
 - (c) Set $\theta_r^{(t)} = \check{\theta}$. For each j in $\{1, \dots, p\}$

IF $\check{\delta}_j = 1$

we flip it to 0 with probability $\min(1, e^{\tau_{rj} + \theta_{rj} [X(r)]'_{\cdot j} \Omega [X(r)]_{\cdot j}})$

ELSE

flip it to 1 with probability $\min(1, e^{-\tau_{rj}})$.

Here τ_{rj} is as defined in (23). Set $\delta_r^{(t)} = \check{\delta}$.

4 Simulation studies

We first present a comparison of the performance of Algorithms 1 and 2 in terms of relative error and time complexity using a logistic regression with different sample sizes (n) and dimension (p) of the parameter of interest. Secondly we generate data from Ising model with two different structures of θ and compare the error rates and recovery of the quasi-posterior samples for different data size (n). Lastly to show scalability of the algorithm, we construct credible intervals based on the posterior samples for a network parametrized by a large 300×300 matrix θ based on 2000 observations and check the percentage of active parameters that are covered by the credible intervals.

4.1 Comparison of PG and MALA for logistic regression

We first present results comparing the two algorithms based on logistic regression in Figure 1. The data was generated based on a parameter $\theta_\star \in \mathbb{R}^p$ which had 10 active signals of absolute strength approximately $4\sqrt{10\frac{\log(p)}{n}}$ with a positive or negative sign randomly assigned to them. The regressors were drawn from independent Gaussian distribution and adjusted to have $\|X_j\|_2^2 = n$, $j = 1, \dots, p$. We used $\rho = \sqrt{\frac{n}{\log(p)}}$, $\gamma = \frac{1}{n\sqrt{p}}$ and $u = 2$. We define the relative error and recovery as follows

$$\text{relative error at iteration } t : e^{(t)} \stackrel{\text{def}}{=} \frac{\|\theta^{(t)} - \theta_\star\|_2}{\|\theta_\star\|_2} \quad (24)$$

$$\text{F1 score at iteration } t : \text{F1}^{(t)} \stackrel{\text{def}}{=} \frac{2 * TA^{(t)} * PA^{(t)}}{TA^{(t)} + PA^{(t)}} \quad (25)$$

Here,

$TA^{(t)}$ = proportion of true active out of predicted active elements of δ at iteration t and

$PA^{(t)}$ = proportion of predicted active out of truly active elements of δ at iteration t .

We run both algorithm for 5000 iterations. Figure 1 shows the relative error (averaged over the number of iterations), as well as the total computation time. We observe that the relative errors from the two samplers remain close. This is expected since the marginal quasi-posterior distribution of (δ, θ) is the same in both algorithms. The notable conclusion is that the time complexity for the Polya-Gamma sampler degrades compared to the MaLa sampler when the sample size n is much larger than the dimension. This is due to the fact that sampling n Polya-Gamma variables at each iteration increases the computation cost of the algorithm significantly.

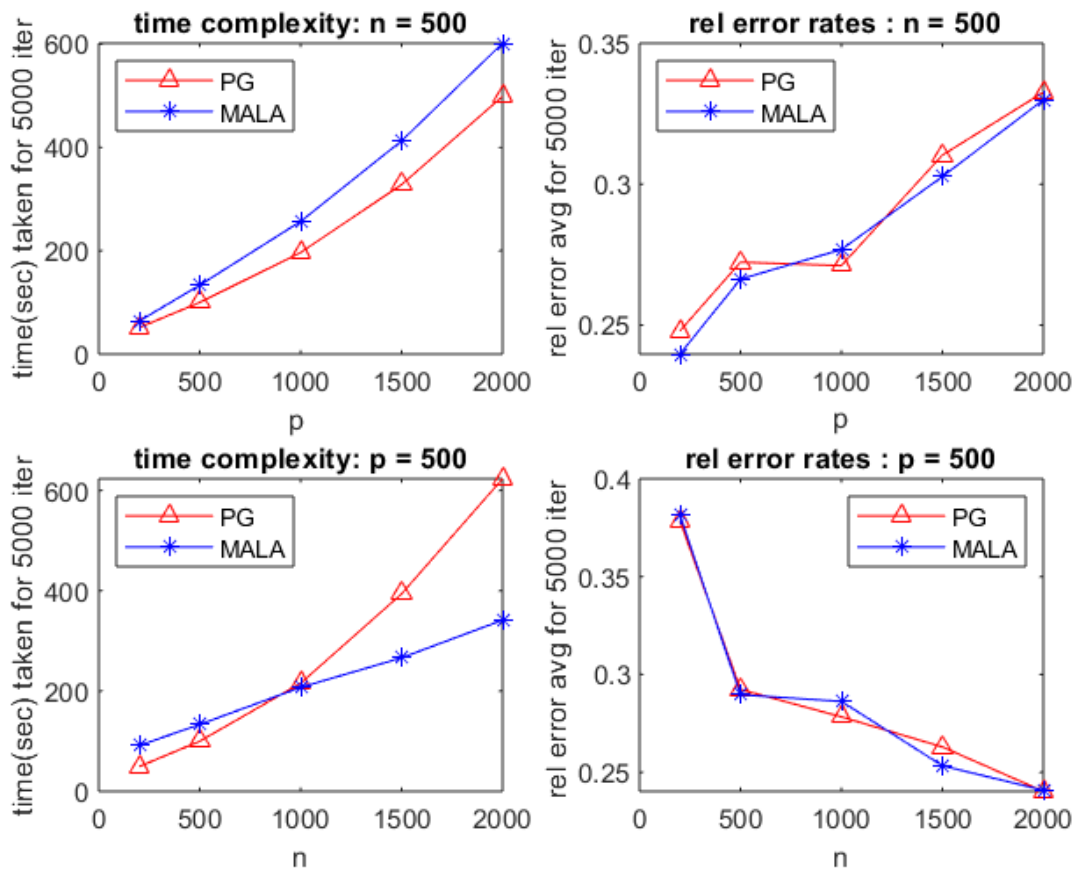


Figure 1: Comparison of MALA 1 and PG 2 for Logistic Regression based on 5000 iterations

4.2 Numerical experiments using the Ising model

The next set of results are based on the whole Ising Model. Here we present results based on two networks, one where the structure is completely random (Figure 2) and the other where it consists of clusters along the diagonals (Figure 3).

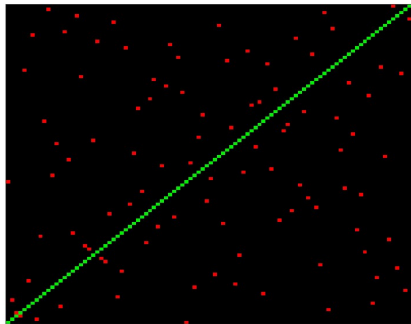


Figure 2: Heatmap of θ_* for network 1

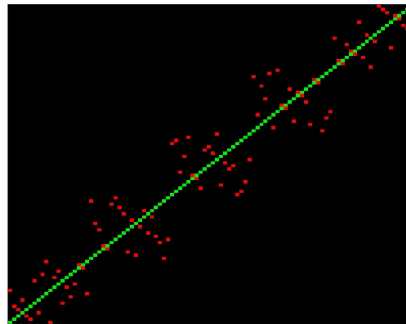


Figure 3: Heatmap of θ_* for network 2

The red and green dots indicate positive and negative values of θ_{ij} respectively

We introduce the norm $\|\theta\|_0$ as a measure of sparsity where

$$\|\theta\|_0 = \sum_{r=1}^p \sum_{j=1}^p \mathbb{1}[\theta_{rj} \neq 0].$$

For each of the two networks, the generating matrix θ_* is symmetric in $\mathbb{R}^{100 \times 100}$. Both the networks have 100 non-zero values along the diagonal of θ_* and 50 active edges out of 4950 edges, resulting in $\|\theta_*\|_0 = 200$.

The Ising model is well known to exhibit a phase transition phenomenon Georgii (1988). The phase transition properties of the Ising model may lead to nodes on graph with low or no variability for certain choices of parameter θ_* Li and Zhang (2010). We carefully chose θ_{*ij} to avoid these scenarios. The diagonal elements of θ_* were chosen to be -2 and the

non-zero off-diagonal θ_{*ij} 's to be 4. We generate the data from the Ising model using a Gibbs sampler.

The initialization of the MCMC values can be done randomly but the mixing will be much slower in this case. We choose to use the frequentist estimate as initial value at each node r obtained through a proximal gradient descent on the corresponding conditional likelihood Parikh and Boyd (2013). This ensures that the MCMC sampler converges almost immediately. As we noted in Figure 1 the PG and MALA sampler produce similar error rates for logistic regression. Hence we present the results of the PG sampler only in case of the Ising Model for the sake of brevity.

To measure convergence of the MCMC we use the relative error (24) for each node r referring to then as $e_r^{(t)}$ for the t_{th} iteration and define

$$\text{relative error at iteration } t \text{ averaged across nodes : } e^{(t)} \stackrel{\text{def}}{=} \frac{\sum_{r=1}^p e_r^{(t)}}{p},$$

Similarly, using (25)

$$\text{F1 score at iteration } t \text{ averaged across nodes : } \text{F1}^{(t)} \stackrel{\text{def}}{=} \frac{\sum_{r=1}^p \text{F1}_r^{(t)}}{p}.$$

F1 score is the combined measure of the power of a method and it's control over false discoveries. A high F1 score indicates low type 1 error and high power.

4.3 Behavior of the quasi-posterior distribution with increasing sample size

We study here the behavior of the quasi-posterior distribution as the sample size increases. We generate n independent samples from the Ising model with parameter $\theta_* \in \mathbb{R}^{100 \times 100}$, for $n \in \{200, 500, 1000\}$, where θ_* is as described above. Using the simulated data, we ran the

PG sampler for 5,000 iterations with $\gamma = \frac{0.1}{p}$, $\rho = \sqrt{\frac{n}{\log(p)}}$ and $u = 2$. We initialize the PG sampler using the frequentist lasso estimate. The relative errors and F1 scores averaged both over the nodes and the last 1,000 iterations are presented in Table 1. We can see a substantial increase in performance when the sample size grows from 200 to 500 and there is not much gain in terms of precision of estimate as sample size is increased further to 1,000. The quasi-Bayesian approach appears to perform equally well for the two types of network.

		Average Relative Error	Average F1 score
Network 1 $p = 100$	$n = 200$	0.2187	0.9336
	$n = 500$	0.0992	0.9960
	$n = 1,000$	0.0704	0.9955
Network 2 $p = 100$	$n = 200$	0.1698	0.9689
	$n = 500$	0.0846	1.0000
	$n = 1,000$	0.0690	0.9960

Table 1: Table showing average relative errors and average F1 scores (recovery) for the two networks and different sample sizes.

4.4 Behavior of credible intervals for a network with 300 nodes

We generate a larger network with 300 nodes and 2,000 observations. The network structure is similar to network 2 with block structure along the diagonals but also some sparse active edges along the anti-diagonal resulting in $\max_{r=1,\dots,p} \|\delta_{*r}\|_0 = 3$. Here θ_* is symmetric in $\mathbb{R}^{300 \times 300}$ with $\|\theta_*\|_0 = 660$. The non-zero off-diagonal values of θ_* are set at 4 and the diagonals of θ_* are either -2 or -4 . The settings were changed slightly again keeping in mind the phase transition properties of the Ising Model. In this setup, we specifically look at the credible intervals estimated through the MCMC samples using the PG sampler with $\gamma = \frac{0.1}{p}$, $\rho = \sqrt{\frac{n}{\log(p)}}$ and $u = 2$. We run the PG sampler for 30,000 iterations and take

the initial 10,000 iterations as burn-in. After the burn-in, the estimates of each θ_{ij} are obtained by taking the mean of 500 samples, keeping the sample from every 40th iteration. The relative error for these 500 samples averaged across the 300 nodes is **0.0078** while the recovery(F1 score) is calculated to be **1.0000**. We obtain the final estimate of $\tilde{\theta}$ after symmetrization of the estimates as mentioned in (9). For the credible interval of θ_{*ij} we use the union of the 95% credible intervals of θ_{ij} and that of θ_{ji} . Figures 4 and 5 show the credible intervals of the active and inactive θ_{ij} separately. We also include the estimates and the true value of the parameter to show the accuracy of the estimates. In 97% cases the active parameters are covered by the union credible intervals while in 3% cases they fall just outside. The inactive parameters have credible intervals symmetric around 0. The average credible intervals for each of the 4 distinct true parameter values are given in table 2 .

True parameter value	Average Credible Interval
0	(-0.037,0.037)
-4	(-4.43,-3.62)
-2	(-2.21,-1.82)
4	(3.66,4.40)

Table 2: Table showing Credible Intervals average for each of the four unique parameter values in the matrix θ_*

The total computing time of our method for this network with 300 nodes and 2000 observations was approximately 600 CPU-hours where each node ran for 30000 iterations. We parallelized the MCMC into 80 parallel processes and the simulation was completed in approximately 8 hours. Given this, we can say that our method is computationally scalable in these data dimensions.

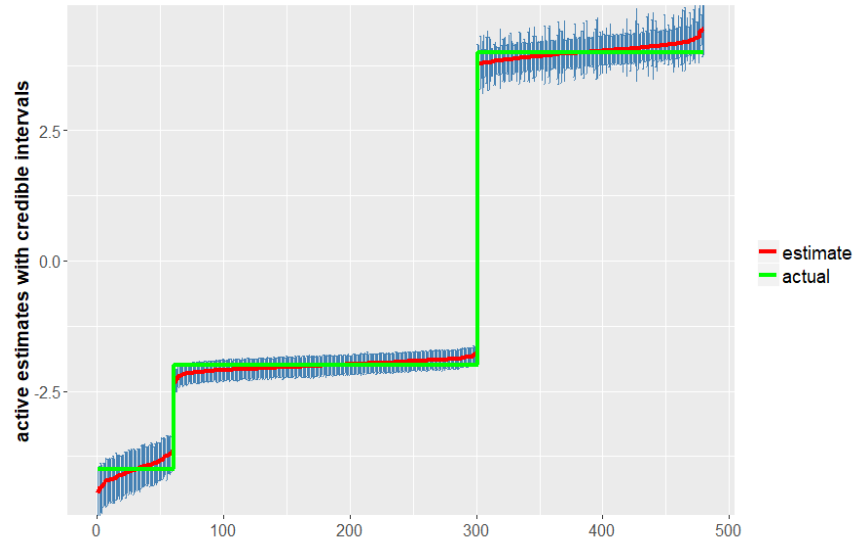


Figure 4: Credible intervals of active θ_{ij} in order of strength of estimates

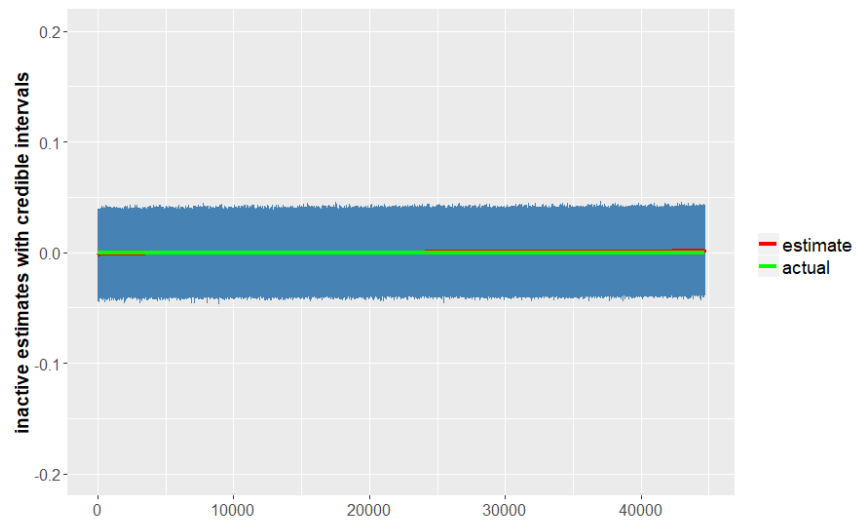


Figure 5: Credible intervals of inactive θ_{ij} in order of strength of estimates

5 Real data analysis

According to British psychologist Raymond Cattell, variations in human personality is best explained by a model containing sixteen variables (personality factors/traits) Cattell and Mead (2008). The data that we have analyzed (source: https://openpsychometrics.org/_rawdata/), comes from an interactive questionnaire of 163 questions designed to measure Cattell's 16 Personality Factors (16PF). For each question, a self-assigned score indicates how accurate it is on a scale of (1) disagree (2) slightly disagree (3) neither agree nor disagree (4) slightly agree (5) agree. Additionally, some other information is collected which includes the test taker's home country, the source from which (s)he got information about the test, her/his perceived accuracy about the answers (s)he provided, age, gender and time elapsed to complete the test. In our analysis, we focused on women in the age group of 30 to 50, who had a self-reported accuracy $\geq 75\%$ and finished the test within half an hour.

The selected data had 4,162 individuals answering 163 questions. Some of the observations had missing values which are represented as 0. The proportion of missing values varied from 0.4% to 1% across different questions. The missing values were treated as missing at random and each of them were substituted by a value between 1 to 5. This value was sampled from the marginal distribution of scores for that particular question (covariate).

Table 3 describes the 16 primary factors. Each factor has 10 questions associated with it except trait B (Reasoning) which has 13 questions leading to a total of 163 questions.

Trait Name	Trait Code
Warmth	A
Reasoning	B
Emotional Stability	C
Dominance	E
Liveliness	F
Rule-Consciousness	G
Social Boldness	H
Sensitivity	I
Vigilance	L
Abstractedness	M
Privateness	N
Apprehension	O
Openness to change	Q1
Self-reliance	Q2
Perfectionism	Q3
Tension	Q4

Table 3: 16 PF Primary Factors

We aim to model the network of 163 questions through a Potts model with 163 nodes. Each of the questions are evaluated on a scale of 1 to 5, resulting in a 5-colored Potts model. Our objective is to understand the associations between the questions by estimating the parameter matrix θ in the Potts model (1). We set the coupling function $C(z_r, z_j) = \frac{z_r z_j}{(4)^2}$ and marginal term $C(z_r) = (\frac{z_r}{4})^2$, where $z_r \in (0, 1, \dots, 4)$ after shifting the origin to 0. The denominators in these terms help stabilize the computation of the log-likelihoods and the derivatives required in our MCMC computations. We run the MALA sampler (Algorithm 1) using $\rho = \sqrt{n/\log(p)}$, $\gamma = \frac{1}{n}$ and $u = 2$, with a burn-in of 10,000 iterations. The

MCMC runs for 50,000 more iterations and we keep every 50_{th} iteration to obtain a 1,000 MCMC samples.

We define

$$\hat{\theta}_{ij} = \frac{1}{1000} \sum_{t=1}^{1000} \theta_{ij}^{(t)} \quad (26)$$

$$\hat{P}(\delta_{ij}) = \frac{1}{1000} \sum_{t=1}^{1000} \mathbb{I}(\delta_{ij}^{(t)} = 0) \quad (27)$$

The final strength of association between node (i, j) based on 1,000 samples is then measured through a single value $\tilde{\theta}_{ij}$ evaluated as in (9) which has values in the range of $(-21, 21)$. The heatmap of the strength of association ($\tilde{\theta}$) is given in Figure 6. The cluster of strong signals around the diagonal represents association between questions relating to the same personality trait while the sparse off-diagonal strong signals represent association between question that are related to two different personality traits. The percentage of estimates with $\hat{P}(\delta_{ij}) = 0$ is around (94%).

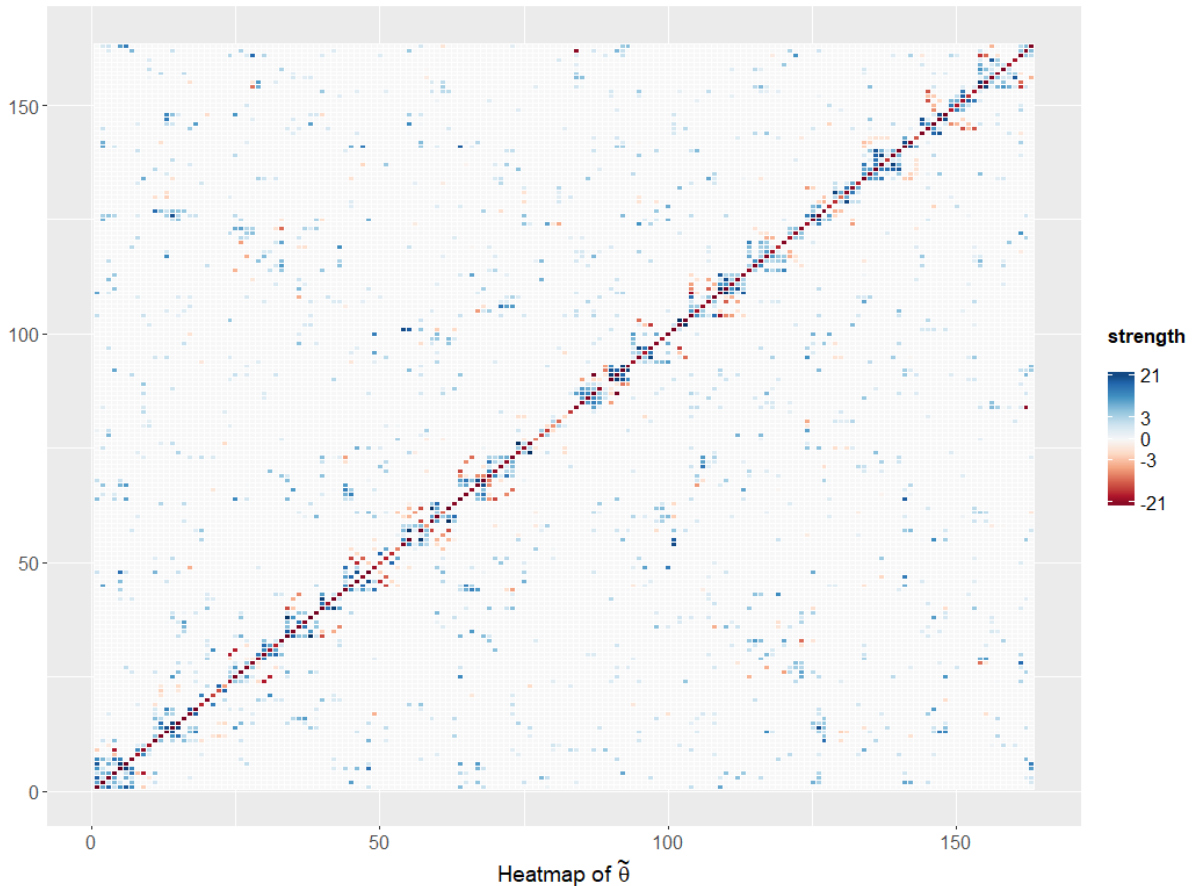


Figure 6: The heatmap of $\hat{\theta}$ after symmetrization (9)

The credible region for the estimate of θ_{ij} are evaluated as union of the 95% credible intervals of θ_{ij} and θ_{ji} , obtained from the respective set of MCMC samples. Figure 7 shows the estimated credible intervals for all the parameters (θ_{ij}). It demonstrates the fact that for most inactive parameters the credible set is a very small interval around 0 which given the scale of the image appears as a straight line. Figure 8 is a zoomed in version of Figure 7 corresponding to parameters whose credible intervals do not contain 0.

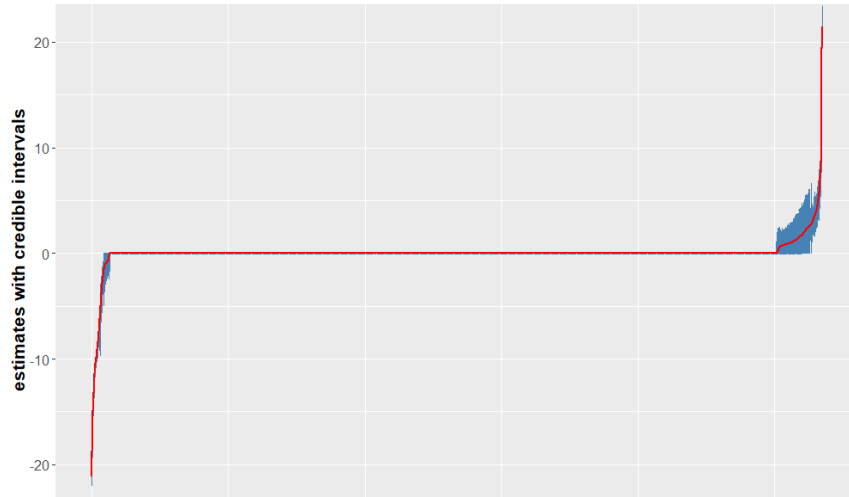


Figure 7: $\tilde{\theta}_{ij}$ (red) with credible intervals (blue) in order of strength of estimates

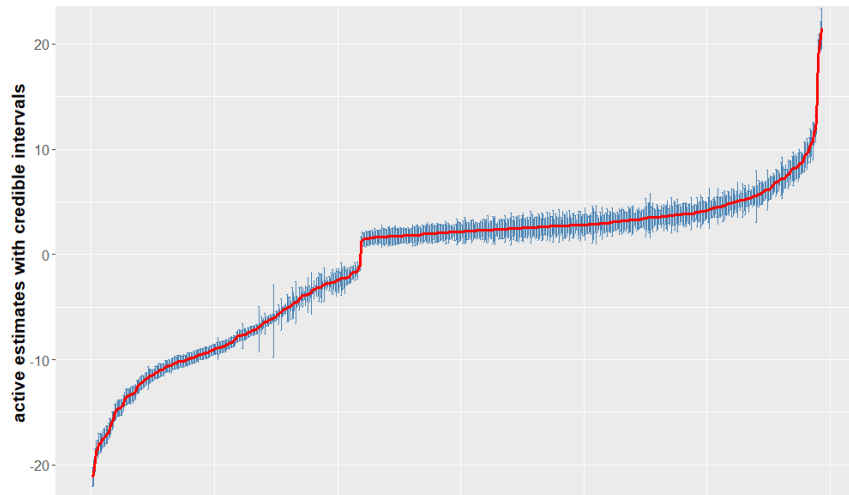


Figure 8: Fig 7 zoomed in for credible intervals not containing 0

We introduce Figure 9 to show the concordance between the estimates $\hat{\theta}_{ij}$ and $\hat{\theta}_{ji}$ for those estimates whose union credible intervals do not contain 0. The figure shows a high level of concordance.

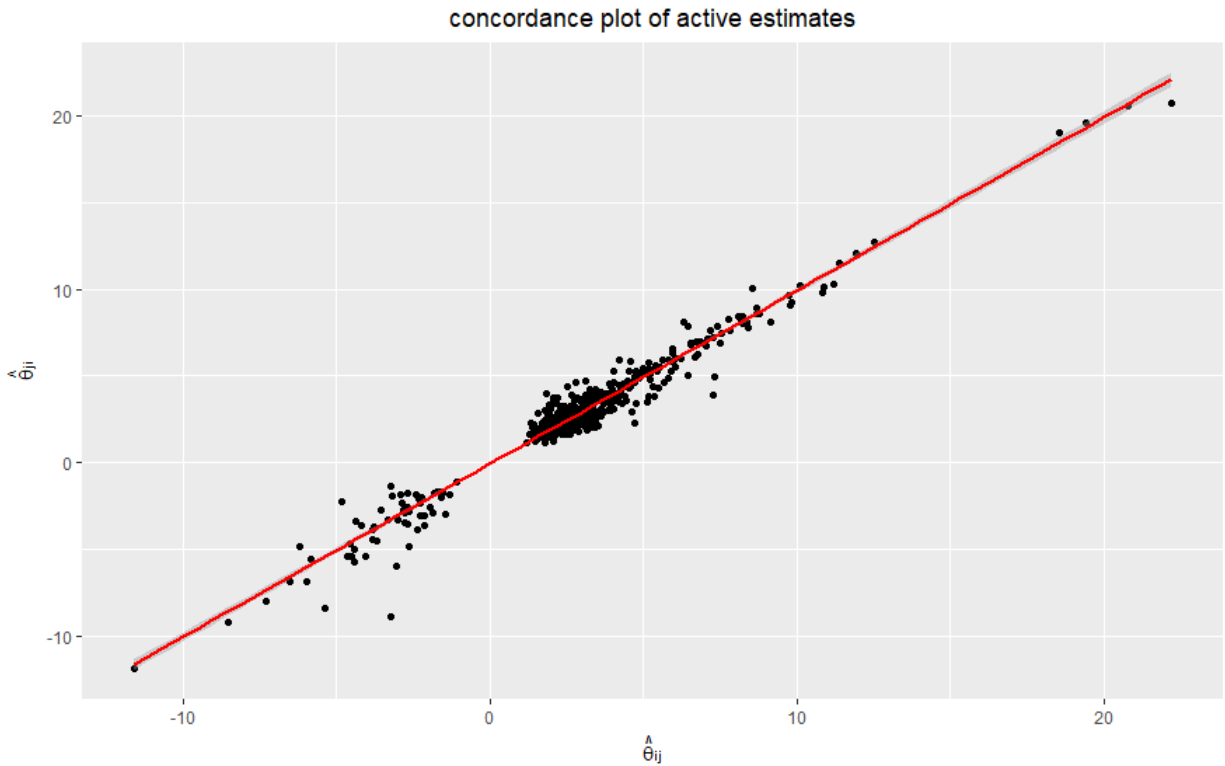


Figure 9: concordance plot for estimates with credible intervals not containing 0. Fitted line in red has intercept: -0.08 and slope: 0.9995

Cattell and Mead (2008) used several techniques including factor analysis to establish that personality structure is hierarchical, with primary and secondary level traits. The primary level consists of the 16 personality traits (used in our analysis). The secondary level consists of a version of the Big Five Traits corresponding to broader human qualities. They are obtained by factor-analyzing the correlation matrix of the 16 primary-level personality traits.

The grouping of the 16 primary factors into the Big Five Traits are shown in Table 4. Reasoning (trait B) stands alone without any association to the Big Five Traits.

Big Five Traits	Associated 16PF Traits
Introversion/Extroversion	A, F, H, N, Q2
Low anxiety/High Anxiety	C, L, O, Q4
Receptivity/Tough-Mindedness	A, I, M, Q1
Accommodation/Independence	E, H, L , Q1
Lack of Restraint/Self Control	F, G, M, Q3
–	B

Table 4: Grouping of the 16 primary factors into the Big Five Traits

With the results of the analysis we now wish to see if the 16 primary factors show similar associations as the ones established in Table 4, thus providing a validation to the inference. In order to do so, we start the probability of edge between the questions (i, j) given by \tilde{p}_{ij} (10) and (27). We summarize the estimates of probability of edge between 163 questions into a smaller 16×16 matrix ϕ corresponding to the 16 traits. We define the set $S_i = \{\text{questions under trait } i\}$ and n_{ij} to be the total number of possible edges between trait i and trait j . We define the matrix ϕ as

$$\phi_{ij} = \frac{1}{n_{ij}} \sum_{k \in S_i, l \in S_j} \tilde{p}_{kl} \quad .$$

The off-diagonal elements of the matrix ϕ measure the average probability of association between each pair of traits. The element-wise reciprocal of this matrix gives us a pseudo-distance measure between the 16 traits which is used to form a hierarchical clustering using Ward’s method (`ward.D2` in `stats:hclust` in R).

Figure 10 shows the results of the clustering. We see that our method perfectly recovers the low-anxiety/high-anxiety (C,L,O,Q4) cluster [Table 4]. It also nearly recovers Introversion/Extroversion (A, H, N, Q2)[Table 4]. The trait F(liveliness) [Table 3] which is

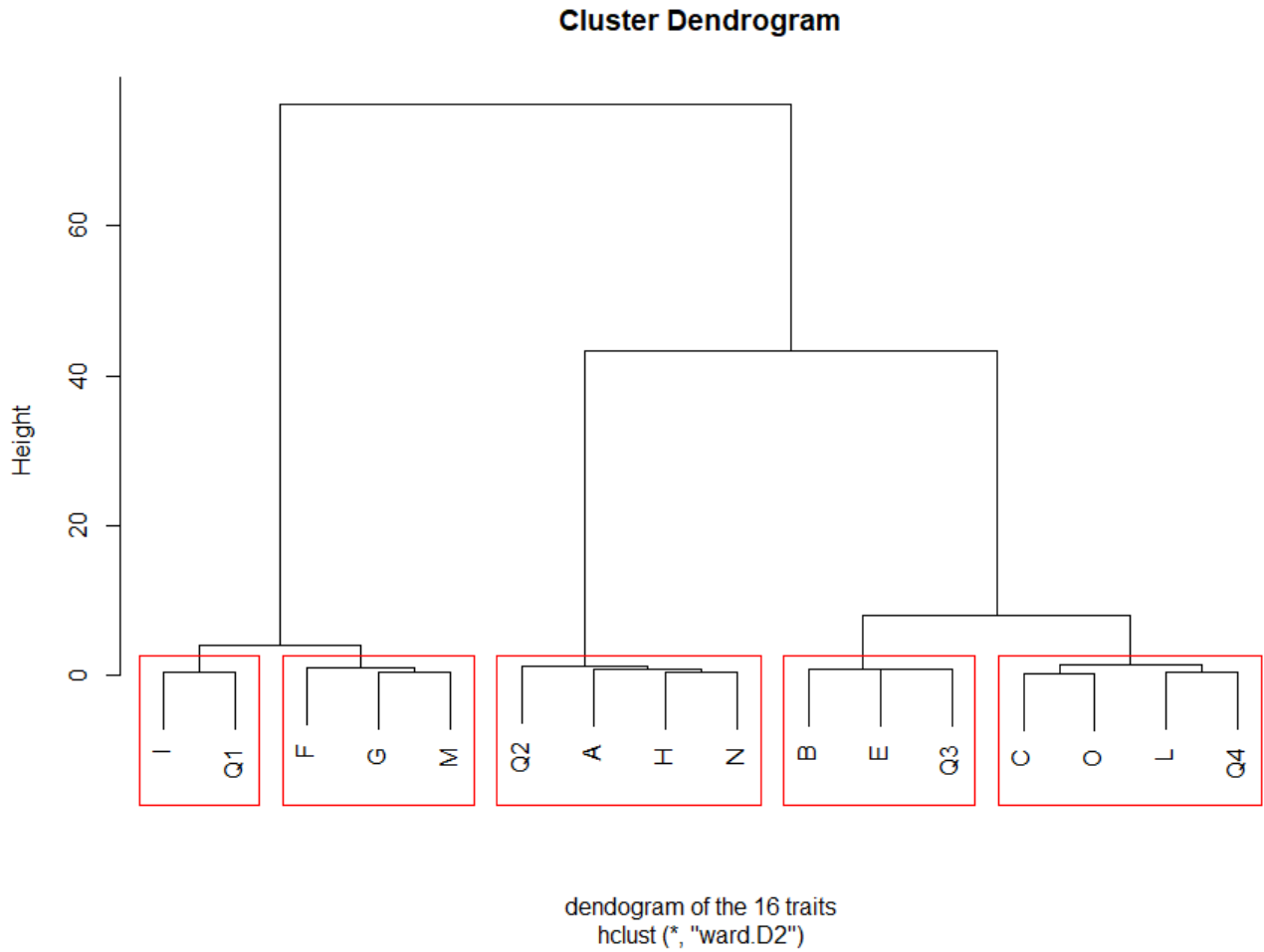


Figure 10: dendrogram identifying clusters of the 16 traits

common to both Introversion/Extroversion and Lack of Restraint/Self-Control in Table 4 is shown to be clustered more strongly with the later group and we also recover most of the Lack of Restraint/Self Control Cluster (F,G,M). In our clustering (I,Q1) are also placed together which is substantiated by the fact that they are common to the Receptivity/Tough-Mindedness cluster [Table4]. Additionally we find that given the data and the demographics with which we chose to work our method identifies a new cluster (E,Q3,B) which may lead to possible novel insights for this particular demographic warranting further investigations. Thus we see that several groupings in Table 4 corresponding to the Big Five Traits are reflected in our method.

6 Conclusion

In this article, we have developed a quasi-Bayesian approach to fit large Potts models. The use of a pseudo-likelihood and a prior distribution that factorizes across the columns of the parameter matrix has enabled us to side-step the intractable normalization constant of the Potts model and perform computations in parallel for each node of the graph. We have shown in our simulations that for appropriate choices of the hyper-parameters, the method recovers the true data-generating parameters and achieves high F1 scores for moderate sample size. We have also shown that the proposed MCMC algorithms can easily handle problem sizes up to $p = 300$, and possibly more if access to a computer with a large number of cores is available. Finally we have implemented the method on a 16 Personality Factor dataset and shown through a hierarchical clustering of our estimates that some of the important features of association between the 16 Personality Factors in captured in our estimates thus validating our inference. The proposed quasi-Bayesian approach has also good theoretical properties as explored in Atchade and Bhattacharyya (2019).

SUPPLEMENTARY MATERIAL

Matlab-code: The matlab package with readme file is located at https://github.com/anwshaumich/DGM_parcomp

16PF data set: The Data set used for analysis in section 5 can be obtained from https://github.com/anwshaumich/DGM_parcomp/blob/master/16PF_data_used.zip. The data has been filtered to consider women between age between 30 to 50, self-reported accuracy of 75 or above and completion time less than half hour ("smalldat.csv"). After adjusting for the missing data we have the dataset "distmiss.csv".

References

- Atchade, Y. (2017). On the contraction properties of some high-dimensional quasi-posterior distributions. *Annals of Statistics* 45, 2248–2273.
- Atchade, Y. (2019). Quasi-bayesian estimation of large gaussian graphical models. *Journal of Multivariate Analysis* 173, 656–671.
- Atchade, Y. and A. Bhattacharyya (2019). An approach to large-scale quasi-bayesian inference with spike-and-slab priors. *Arxiv*.
- Atchade, Y. F. (2006). An adaptive version for the metropolis adjusted langevin algorithm with a truncated drift. *Methodol. Comput. Appl. Probab.* 8, 235–254.
- Banerjee, O., L. El Ghaoui, and A. d’Aspremont (2008). Model selection through sparse maximum likelihood estimation for multivariate gaussian or binary data. *J. Mach. Learn. Res.* 9, 485–516.
- Banerjee, S. and S. Ghosal (2015). Bayesian structure learning in graphical models. *Journal of Multivariate Analysis* 136, 147 – 162.
- Besag, J. (1974). Spatial interaction and the statistical analysis of lattice systems. *J. Roy. Statist. Soc. Ser. B* 36, 192–236.
- Cattell, H. and A. Mead (2008). Personality measurement and testing. *The SAGE Handbook of Personality Theory and Assessment* 2, 133–159.
- Chernozhukov, V. and H. Hong (2003). An MCMC approach to classical estimation. *J. Econometrics* 115(2), 293–346.
- Dobra, A., A. Lenkoski, and A. Rodriguez (2011). Bayesian inference for general gaussian graphical models with application to multivariate lattice data. *Journal of the American Statistical Association* 106, 1418–1433.
- Ekeberg, M., C. Lövkvist, Y. Lan, and E. A. M. Weigt (2013). Improved contact prediction in proteins: Using pseudolikelihoods to infer potts models. *Physical Review* 87.
- Epskamp, S., D. Borsboom, and E. Fried (2018). Estimating psychological networks and their accuracy: A tutorial paper. *Behavior research methods* 50.
- Epskamp, S., J. Kruijs, and M. Marsman (2017). Estimating psychopathological networks: Be careful what you wish for. *PLoS ONE* 12.
- George, E. I. and R. E. McCulloch (1997). Approaches to bayesian variable selection. *Statistica Sinica* 7, 339–373.
- Georgii, H.-O. (1988). Gibbs measures and phase transitions. *de Gruyter Studies in Mathematics* 9.

- Greenfield, A., C. Hafemeister, and Bonneau, R. (2013). Robust data-driven incorporation of prior knowledge into the inference of dynamic regulatory networks. *Bioinformatics* 29, 1060–1067.
- Guo, J., J. Cheng, E. Levina, G. Michailidis, and J. Zhu (2015, 06). Estimating heterogeneous graphical models for discrete data with an application to roll call voting. *Ann. Appl. Stat.* 9(2), 821–848.
- Guyon, X. (1995). *Random fields on a network*. Probability and its Applications (New York). New York: Springer-Verlag. Modeling, statistics, and applications, Translated from the 1992 French original by Carenne Ludeña.
- Höfling, H. and R. Tibshirani (2009, 04). Estimation of sparse binary pairwise markov networks using pseudo-likelihoods. *Journal of machine learning research : JMLR* 10, 883–906.
- Ising, E. (1925). Beitrag zur theorie des ferromagnetismus. *Zeitschrift Für Physik A Hadrons and Nuclei* 31, 253–258.
- Jiang, W. and M. A. Tanner (2008). Gibbs posterior for variable selection in high-dimensional classification and data mining. *Ann. Statist.* 36(5), 2207–2231.
- Kato, K. (2013). Quasi-bayesian analysis of nonparametric instrumental variables models. *Annals of Statistics* 41, 2359–2390.
- Khondker, Z. S., H. Zhu, W. Chu, H. and Lin, and J. G. Ibrahim (2013). Bayesian covariance lasso. *The Stat. Interface* 6, 243–259.
- Li, C. and W. Jiang (2014, May). Model Selection for Likelihood-free Bayesian Methods Based on Moment Conditions: Theory and Numerical Examples. *ArXiv e-prints*.
- Li, F. and N. R. Zhang (2010). Bayesian variable selection in structured high-dimensional covariate spaces with applications in genomics. *J. Amer. Statist. Assoc.* 105, 1202–1214.
- Liao, Y. and W. Jiang (2011, 12). Posterior consistency of nonparametric conditional moment restricted models. *Ann. Statist.* 39(6), 3003–3031.
- Liu, J. (2001). Monte carlo strategies in scientific computing. *Springer*.
- Lyne, A., M. Girolami, Y. Atchade, H. Strathmann, and D. Simpson (2015). On russian roulette estimates for bayesian inference with doubly-intractable likelihoods. *Statistical Science* 30, 443–467.
- Meinshausen, N. and P. Bühlmann (2006). High-dimensional graphs with the lasso. *Annals of Stat.* 34, 1436–1462.
- Mitchell, T. J. and J. J. Beauchamp (1988). Bayesian variable selection in linear regression. *J. Amer. Statist. Assoc.* 83, 1023–1032.

- Murray, I., Z. Ghahramani, and D. MacKay (2006). MCMC for doubly-intractable distributions. *Proceedings of the 22nd Annual Conference on Uncertainty in Artificial Intelligence UAI06*, 359–366.
- Narisetty, N. and X. He (2014). Bayesian variable selection with shrinking and diffusing priors. *Annals of Statistics* 42, 789–817.
- Parikh, N. and S. Boyd (2013). Proximal algorithms. *Foundations and Trends in Optimization* 1.
- Peng, B., D. Zhu, B. P. Ander, X. Zhang, F. Xue, F. Sharp, and X. Yang (2013). An integrative framework for bayesian variable selection with informative priors for identifying genes and pathways. *PLoS ONE* 8(7).
- Peterson, C., F. C. Stingo, and M. Vannucci (2015). Bayesian inference of multiple gaussian graphical models. *Journal of the American Statistical Association* 110, 159–174.
- Polson, N., J. Scott, and J. Windle (2013). Bayesian inference for logistic models using poly-gamma latent variables. *Jour. of the Amer. Stat. Assoc.* 108, 1339–1349.
- Ravikumar, P., M. J. Wainwright, and J. D. Lafferty (2010). High-dimensional Ising model selection using ℓ_1 -regularized logistic regression. *Ann. Statist.* 38(3), 1287–1319.
- Robert, C. P. and G. Casella (2004). Monte carlo statistical methods. *Springer Texts in Statistics, Springer-Verlag, New York.*
- Roy, S., Y. Atchadé, and G. Michailidis (2017). Change point estimation in high dimensional markov random-field models. *Journal of the Royal Statistical Society: Series B (Statistical Methodology)* 79(4), 1187–1206.
- Studham, M., A. Tjarnberg, T. Nordling, S. Nelander, and E. Sonnhammer (2014). Functional association networks as priors for gene regulatory network inference. *Bioinformatics* 30, i130–i138.
- Yang, W. and X. He (2012). Bayesian empirical likelihood for quantile regression. *Ann. Statist.* 40(2), 1102–1131.
- Zhou, X. and S. Schmidler (2009). Bayesian parameter estimation in ising and potts models: A comparative study with applications to protein modeling. *Technical Report*.